

Contents lists available at ScienceDirect

Physica D

journal homepage: www.elsevier.com/locate/physd



On the stability of traveling wave solutions to thin-film and long-wave models for film flows inside a tube



Roberto Camassa ^{a,1}, Jeremy L. Marzuola ^{a,1}, H. Reed Ogrosky ^{b,*,1}, Sterling Swygert ^{a,1}

- ^a Department of Mathematics, University of North Carolina-Chapel Hill, Phillips Hall, Chapel Hill, NC 27599, USA
- ^b Department of Mathematics and Applied Mathematics, Virginia Commonwealth University, Harris Hall, Richmond, VA 23284, USA

ARTICLE INFO

Article history:
Received 25 September 2019
Received in revised form 28 August 2020
Accepted 22 September 2020
Available online 28 September 2020
Communicated by T. Grava

Keywords: Thin films Lubrication theory Traveling waves Numerical continuation Asymptotics

ABSTRACT

Traveling wave solutions are studied numerically and theoretically for models of viscous core-annular flows and falling film flows inside a tube. The models studied fall into one of two classes, referred to here as 'thin-film' or 'long-wave'. One model of each type is studied for three problems: a falling viscous film lining the inside of a tube, and core-annular flow with either equal- or unequal-density fluids. In recent work, traveling wave solutions for some of these equations were found using a smoothing technique that removes a degeneracy and allows for continuation onto a periodic family of solutions from a Hopf bifurcation. This paper has three goals. First, the smoothing technique used in earlier studies is justified for these models using asymptotics. Second, this technique is used to find numerically families of traveling wave solutions not previously explored in detail, including some which have multiple turning points due to the interaction between gravity, viscous forces, surface tension, and pressure-driven flow. Third, the stability of these solutions is studied using asymptotics near the Hopf bifurcation point, and numerically far from this point. In particular, a simple theory using the constant solution at the Hopf bifurcation point produces estimates for the eigenvalues in good agreement with numerics, with the exception of the eigenvalues closest to zero; higher-order asymptotics are used to predict these eigenvalues. Far from the Hopf bifurcation point, the stabilizing role of increasing surface tension is quantified numerically for the thin-film models, while multiple changes in stability occur along families of solutions for some of the long-wave models.

© 2020 Elsevier B.V. All rights reserved.

1. Introduction

Core–annular flows and viscous film flows inside a tube arise in a wide variety of engineering, biological, and other scientific applications [1]. Even in the absence of any background flow, the presence of a free surface in such settings results in interesting dynamics due to long-wave instabilities, including plug formation and film breakup.

In the presence of background flow due to, e.g., density differences between the core and annular fluids, and/or active pressure-driven flow, the free-surface dynamics can become quite rich, and these problems are the focus of the current paper. In particular, the problems studied here are (i) the flow of a viscous film coating the interior of a vertical rigid tube of radius \bar{a} , and (ii) core–annular flow; see Fig. 1 for a definition sketch of the flow variables for problem (ii). Since many experiments exhibit

E-mail addresses: camassa@amath.unc.edu (R. Camassa), marzuola@math.unc.edu (J.L. Marzuola), hrogrosky@vcu.edu (H.R. Ogrosky), swygerts@live.unc.edu (S. Swygert). dynamics that are predominantly axisymmetric, an axisymmetric flow is assumed here so that the annular film lies within $\bar{R}(\bar{z},\bar{t})<\bar{r}<\bar{a}$, where \bar{R} represents the film's free-surface. The core region $(0<\bar{r}<\bar{R})$ is filled with a second, much less viscous, fluid that is either passive or is driven up the tube with volume flux \bar{Q} by an imposed pressure gradient. Superscripts of (a) and (c) will be used to denote variables and parameters associated with the annular and core regions, respectively. In the event that (i) the density difference between the two fluids is negligible $(\rho^{(a)}-\rho^{(c)}=0)$, and/or (ii) the core fluid is passive $(\bar{Q}=0)$, some terms of the model equations may be neglected resulting in a simpler model with fewer parameters.

It is well known that the free surface in such problems is unstable to long-wave disturbances; see, e.g., [2–5]. Lubrication theory has been used to derive a variety of strongly nonlinear single-PDE models that have successfully described the evolution of the free surface in these axisymmetric film flows. These strongly nonlinear models are derived by assuming a small ratio of lengthscales and fall into one of two categories. 'Thin-film' models rely on a small film thickness compared with the tube radius [6–8], while 'long-wave' models utilize a small film thickness relative to a typical wavelength of free-surface disturbances

^{*} Corresponding author.

¹ All authors equally contributed to this manuscript.

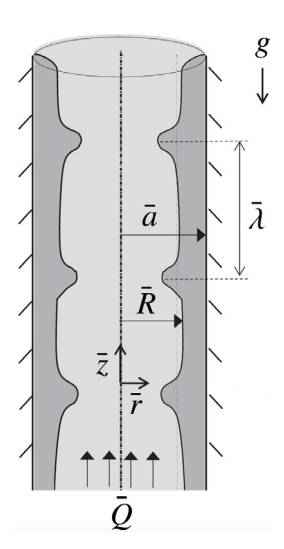


Fig. 1. Definition sketch of the flow variables. $\bar{r}=\bar{R}(\bar{z},\bar{t})$ denotes the location of the free-surface, $\bar{\lambda}$ is a typical free-surface wavelength, \bar{Q} denotes the volume flux of core fluid moving up the tube, and g is acceleration due to gravity.

[9–13]. See [14] for further discussion of this classification in film flows coating a tube. These models display a wide range of free-surface dynamics, including traveling wavetrains, interacting pulses (which have been well-described by systematic coherent-structure theories in various settings [15–20]), chaotic dynamics, and finite-time blow-up. We also note that other modeling approaches have been developed, particularly integral boundary layer models for moderate Reynolds number flows [21–23].

In previous works, these and related model equations have been studied numerically and analytically in order to address a variety of questions regarding linear stability analysis, wave amplitude saturation, interactions between free-surface waves, traveling wave solutions, solitary waves, and the stability of solutions [6–11,14,19,20,24–29]. Due to the nonlinearities in each model (particularly the long-wave models), numerical techniques have been relied upon to find families of traveling wave solutions. One method for finding such solutions is to identify a Hopf bifurcation and continue onto a branch of periodic solutions from the Hopf bifurcation point.

One difficulty, however, is a degeneracy that arises due to the presence of a zero-Hopf bifurcation point (sometimes called a fold-Hopf bifurcation point) in each of these equations; such bifurcations have both a zero eigenvalue and an imaginary pair of eigenvalues [30]. The presence of the zero eigenvalue makes continuation onto a branch of periodic solutions more difficult numerically. In order to make this continuation easier, the degeneracy may be removed by adding a small smoothing term to the equation; once on the periodic branch, the smoothing term may be removed via continuation. This was done in, e.g., [25], and while this technique appears to provide a reasonable route to study families of solutions, no careful justification of the technique on these equations was provided in [25]. Furthermore, the stability of these traveling wave solutions was studied numerically in [10,25] for the case of passive core flow, and it was shown that for combinations of period and parameter values relevant to motivating experiments, all of the traveling wave solutions were unstable.

These results suggest several questions that motivate the current study. Can the smoothing technique used in [25] to find traveling wave solutions be justified analytically? How does including active core flow in the model equations affect the family of solutions (and their stability) found for passive core flow

in [25]? What can be said analytically about the stability of these solutions?

In this paper, a combination of numerical and analytical results are presented to address these motivating questions. First, the smoothing technique used in [25] to remove the degeneracy of the Hopf bifurcation is justified analytically. Second, families of periodic solutions are found for a class of both long-wave and thin-film models; some of these families have multiple turning points not previously reported. Lastly, the stability of these traveling wave solutions is studied near the Hopf bifurcation point using asymptotics, and far from the Hopf bifurcation point numerically. The analytical work is presented primarily for thinfilm equations as their simpler nonlinearities allow for clearer exposition, but in principle the same techniques should also be applicable to their corresponding long-wave equations.

The rest of the paper is organized as follows: the model equations studied here are discussed in Section 2. Families of solutions for these models are found numerically in Section 3 using the smoothing method described above, and justification for this technique is provided in Section 4. The stability of traveling wave solutions far from the Hopf point in several of the models is studied numerically in Section 5, and asymptotic results on the stability of solutions near the Hopf bifurcation is presented in Section 6. Conclusions are given in Section 7.

2. Model equations

We first introduce the six model equations that will be discussed; the derivation of each model may be found in the literature cited. The theoretical work presented in this paper will primarily focus on two of the thin-film models, as their simpler structure allows for more explicit calculations and greater clarity, but we include the remaining models as the tools presented here apply to those models as well.

2.1. Thin-film models

The first three models belong to the 'thin-film' class, and are derived by exploiting an assumed small film thickness relative to tube radius. Each equation is written here in terms of dimensionless film thickness h(z,t)=a-R(z,t), where $a=\bar{a}/\bar{R}_0$. In the case of passive core flow $(\bar{Q}=0)$ with unequal fluid densities, the free-surface dynamics are governed by the model derived by Frenkel [6]:

$$h_t + 2h^2h_z + S[h^3(h_z + h_{zzz})]_z = 0,$$
 (1)

where the parameter S (the inverse of Bond number) encapsulates surface tension effects competing with gravity. Here $S=S_F=2\bar{\sigma}\bar{h}_0/(3\bar{\rho}\bar{g}\bar{a}^3)$ with surface tension $\bar{\sigma}$, mean film thickness \bar{h}_0 , film density $\bar{\rho}$, acceleration due to gravity \bar{g} , and tube radius \bar{a} . In the case of active core flow and negligible density difference, the free surface dynamics are described by the model derived by Kerchman [7]:

$$h_t + hh_z + S \left[h^3 (h_z + h_{zzz}) \right]_z = 0.$$
 (2)

where S can now be viewed as a modified capillary number: $S = S_K = \pi \bar{\sigma} \bar{h}_0^2/(12\bar{\mu}^{(c)}\bar{Q}_c)$, with \bar{Q}_c the volume flux of the core fluid, and $\bar{\mu}^{(c)}$ the dynamic viscosity of the core fluid. Superscripts of (a) and (c) represent the annular and core fluids, respectively. If neither density difference or core flow may be neglected, the following model applies,

$$h_t + hh_z - 2Fh^2h_z + S\left[h^3(h_z + h_{zzz})\right]_z = 0,$$
 (3)

where $F = \pi(\bar{\rho}^{(a)} - \bar{\rho}^{(c)})\bar{g}\bar{a}^3\bar{h}_0/(8\bar{\mu}^{(c)}\bar{Q}_c)$ and $S = S_K$. In the limit $F \to 0$, Eq. (2) may be recovered, and we note that the term h^2h_z appears at higher-order in the asymptotics than the hh_z

term (i.e., for thin films, the effects of the core flow are dominant relative to the effects of gravity on the free-surface evolution).

Each of Eqs. (1)–(3) is a conservation law for film thickness h, and linear stability analysis shows that each of these equations has a constant solution that is unstable to long-wave disturbances. Solutions to (1) were studied numerically by Kerchman and Frenkel [28]: simulations show a rich variety of wave dynamics and traveling wave solutions were found for a variety of parameter values S and period. In [27], Kalliadasis and Chang studied the existence of solitary wave solutions to (1) and found a critical thickness that could determine whether finite-time blowup of solutions could be expected. Note that in the absence of a base flow, Eq. (1) reduces to the equation derived by Hammond [31]. Numerical solutions to (2) were studied by Kerchman in [7] for a variety of values of S and period, and we note that (2) can be reduced to the Kuramoto-Sivashinsky equation [32-34]. We also note that the same equation has been derived for Taylor-Couette flow, but where the independent variable is an angle, θ , rather than the height z; thus different boundary conditions apply in this setting [35].

Lastly, we stress that the notation S is used in each of (1)–(3), but has a different definition in terms of physical quantities for each equation.

2.2. Long-wave models

Each of (1)–(3) has a corresponding long-wave model that is applicable in the event that the film thickness is not necessarily small relative to the tube radius. For passive core flow, the model studied in [10,25] applies,

$$R_t - f_2(R; a)R_z + \frac{\tilde{S}}{R} [\tilde{f}_3(R; a)(R_z + R^2 R_{zzz})]_z = 0, \tag{4}$$

where

$$f_2(R; a) = a^2 - R^2 - 2R^2 \log\left(\frac{a}{R}\right),$$

$$\tilde{f}_3(R; a) = \frac{1}{a^2} \left[\frac{a^4}{R^2} - 4a^2 + 3R^2 + 4R^2 \log\left(\frac{a}{R}\right) \right],$$

and where the dynamics are governed by the film thickness parameter $a=\bar{a}/\bar{R}_0$ and $\tilde{S}=3\bar{a}S_F/(16\bar{h}_0)$. (We note that \tilde{S} is a rescaled version of the parameter S used in [14], with $\tilde{S}=a^2S$, so that S does not depend on film thickness but only on the 'hardware' parameters like density, viscosity, etc.). This model is nearly identical to the one derived by [26] to study a falling film on the exterior of a tube.

For negligible density difference, the model derived in [14,24] applies,

$$R_t + f_1(R; a)R_z + \frac{\tilde{S}}{R} [\tilde{f}_3(R; a)(R_z + R^2 R_{zzz})]_z = 0,$$
 (5)

where

$$f_1(R; a) = \frac{a^2}{R^4} \left(\frac{a^2}{R^2} - 1 \right),$$

and where $\tilde{S} = 3\bar{a}^2 S_K/(8\bar{h}_0^2)$.

Finally, if neither density difference or core flow may be neglected, the model derived in [9] applies,

$$R_{t} + [f_{1}(R; a) - \tilde{F}\tilde{f}_{2}(R; a)]R_{z}$$

$$+ \frac{\tilde{S}}{R}[\tilde{f}_{3}(r; a)(R_{z} + R^{2}R_{zzz})]_{z} = 0,$$
(6)

and where

$$\tilde{f}_2(R; a) = \frac{1}{a^4} \left[a^2 - R^2 - 2R^2 \log \left(\frac{a}{R} \right) \right],$$

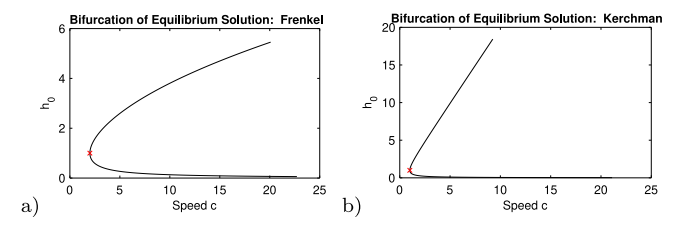


Fig. 2. Family of equilibrium solutions shown in $c - h_0$ space for (a) Eq. (1) and (b) Eq. (2). Red \times denotes a Hopf bifurcation.

$$\tilde{f}_3(R; a) = \frac{1}{a^2} \left[\frac{a^4}{R^2} - 4a^2 + 3R^2 + 4R^2 \log \left(\frac{a}{R} \right) \right],$$

and where $\tilde{F}=2\bar{a}F/\bar{h}_0=\pi(\bar{\rho}^{(a)}-\bar{\rho}^{(c)})\bar{g}\bar{a}^4/(4\bar{\mu}^{(c)}\bar{Q}^{(c)})$ and $\tilde{S}=3\bar{a}^2S_K/(8\bar{h}_0^2)$. Similar to F in (3), in the limit $\tilde{F}\to 0$, Eq. (5) is recovered. We note that each of (4)–(6) contains a parameter \tilde{S} , but that this parameter is uniquely defined in terms of physical constants for each equation.

The thin-film Eqs. (1)–(3) may be recovered from (4)–(6) in the appropriate thin-film limit, and as with the thin-film counterparts, each of the Eqs. (4)–(6) has a constant solution that is unstable to long-wave disturbances (with the wavelength of maximum growth rate determined by the mean location of the free-surface). In contrast to Eqs. (1)–(3), each of the long-wave models (4)–(6) is a conservation law for R^2 , so that the volume of annular fluid, rather than mean film thickness, is conserved. Significantly different dynamics can occur in the thin-film and long-wave models, even for moderate thickness; see [14] for a discussion of differences in wave dynamics, absolute and convective instability, plug formation, streamlines within the film, and other features which may differ qualitatively between the two classes of models.

The theoretical results in Sections 4 and 6 will focus primarily on Eqs. (1) and (2). The simple structure of these equations allows for simpler calculations, but the theoretical tools used here apply equally to the remaining models. Additional numerical results will be given for Eq. (6), as there are interesting features in the families of solutions and their stability that are not present in the other equations.

3. Hopf bifurcations and periodic solutions: numerics

Traveling wave solutions to each of (1)–(6) may be found by substituting h(z,t) = H(Z) (or R(z,t) = Q(Z)), where Z = z - ct with c the wave speed, into the PDE to obtain a fourth-order ODE in Z. Since each equation is a conservation law, these ODEs may be integrated once to obtain a third-order ODE with a constant of integration K that becomes an additional parameter in the problem. For example, for Eq. (2), this third-order ODE is

$$-ch + \frac{1}{2}h^2 + Sh^3(h' + h''') = K, (7)$$

Each of the models (1)–(3) has a family of constant solutions $h(z,t) = h_0$ where h_0 depends on K, c, and F; e.g., for (7), constant solutions must satisfy $-ch + h^2/2 = K$. Similarly each model (4)–(6) has a family of constant solutions $R(x,t) = R_0$ where R_0 depends on K, c, a and F. Fig. 2 shows the parameter space of this family of constant solutions for fixed K = -4/3 for Eq. (1), and for K = -1/2 for Eq. (2); these choices of K produce a zero-Hopf bifurcation at h = 1.

The fact that these Hopf bifurcations are degenerate makes numerical continuation off the Hopf point more difficult. One approach to removing the degeneracy is to add a small viscosity term to the third-order ODE. This approach was used on Eq. (4)

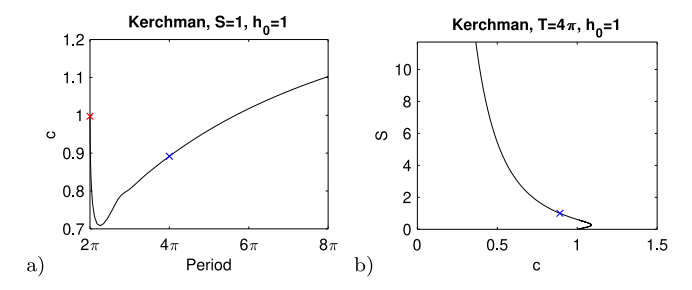


Fig. 3. (a) Family of periodic solutions to (2) with S=1, $h_0=1$, and varying period. (b) Family of periodic solutions to (2) with $h_0=1$, period 4π and varying S=1

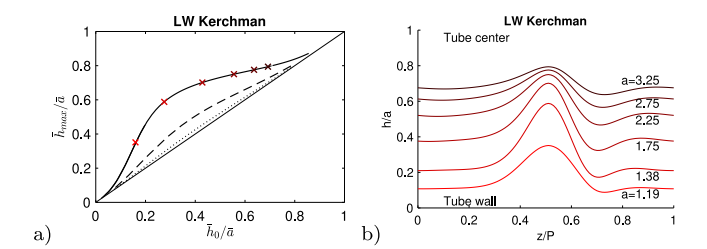


Fig. 4. (a) Family of solutions to (5) with period 4π , $h_0=1$, and various values of a; S=14.9 (solid), S=4.0 (dashed), and S=1.0 (dotted) shown. Red \times 's denote solutions shown in right panel. (b) Periodic solutions to Eq. (5) for various values of $a=\bar{a}/\bar{R}_0$. Period of 4π has been rescaled to 1; h has been rescaled to take on values from 0 (tube wall) to 1 (tube center).

in [25] (and was also used in [36], and discussed in [7]), and is used again here on the remaining five equations. We briefly review this method with Eq. (2), for which the smoothed ODE is

$$-ch + \frac{1}{2}h^2 + Sh^3(h' + h''') + \beta h'' = K,$$
(8)

where $\beta > 0$ represents a small viscosity that removes the degeneracy, resulting in a pure Hopf bifurcation. A family of periodic solutions is obtained from this Hopf point using the continuation software *AUTO* [37], and once on this branch of solutions, we take $\beta \rightarrow 0$ to limit to a family of solutions to the original equation. Fig. 3 shows the parametric representation of this family of solutions for S = 1 and mean thickness $h_0 = 1$ (letting K vary as needed to enforce this integral condition).

Analytically proving that we may satisfactorily compute the $\beta \to 0$ branch once we have properly bifurcated off the degenerate Hopf bifurcation is an open problem that is beyond the scope of this article but hopefully a topic of future study. Near the Hopf bifurcation, this requires using singular perturbation theory to prove that the corresponding linear operator is properly invertible such that one may bifurcate in β using the standard Lyapunov–Schmidt methods.

Fig. 4 shows solutions to (5) for three different values of S, fixed period 4π , and various values of a; see [14] for additional information about these families of solutions. In contrast, in [10, 25] families of solutions to (4) were shown to have a turnaround point, or fold point. This turnaround point appeared to be an indication of a critical thickness that separated a liquid-plug-forming regime from a non-plug-forming regime; see also [38] for some recent results on plug formation in a different model.

Fig. 5 shows the parametric location of families of solutions to Eq. (6), which is essentially a combination of the two Eqs. (5) and (4), though now with the two hyperbolic terms having opposite sign from one another. For small \tilde{F} , families of solutions resemble those of Fig. 4; for some critical \tilde{F} , however, multiple turnaround points appear, creating families of solutions that look

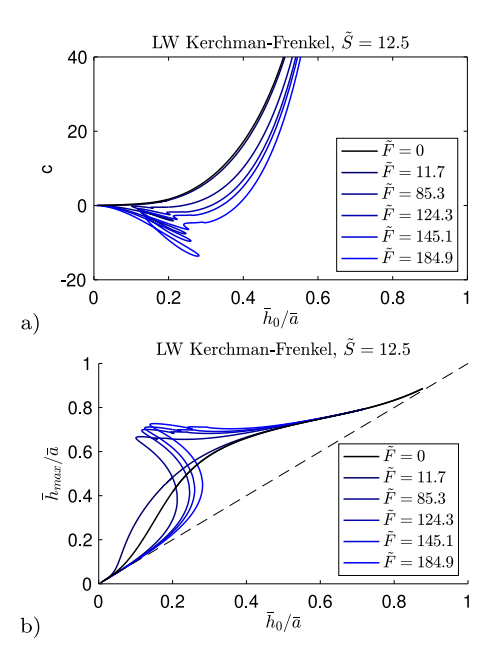


Fig. 5. (a) Families of periodic solutions to Eq. (6) with $\tilde{S} \approx 12.5$ and various values of \tilde{F} and a. (b) Families of periodic solutions to Eq. (6) in $\bar{h}_{max} - \bar{h}_0$ space.

like a blend of solutions to (4) and (5). These families create the possibility of hysteresis in the behavior of solutions, whereby a traveling wave solution may disappear if the film thickness is modified. Profiles of some of these solutions are shown in Section 5.

We note that additional traveling wave solutions have been previously found for some of these models, including solutions with multiple humps; see, e.g., [7] and [25] for such solutions in Eqs. (2) and (4), respectively. However, since both numerical studies and experiments have consistently suggested that single-hump waves are the dominant feature seen in the evolution of the free-surface in these problems, we focus exclusively on single-hump solutions in this paper and leave study of other types to future work [7,9,10].

4. Solutions near Hopf bifurcations for thin film models: asymptotics

We next establish the validity of the smoothing procedure used to find solutions numerically to thin-film Eqs. (1) and (2). Our focus in this section is on the simplified thin-film models to give a clear picture of the degenerate Hopf structure and the means by which to successfully bifurcate using our algorithms. However, we note that similar methods can be applied to each of our models. To this end, we perform a first order, normal form analysis as prescribed in [30], but to implement the procedure we need to choose carefully the parameters for bifurcation. To lay out the procedure, we begin with Eq. (2) (and the corresponding ODE (7)) and consider the system given by

$$\psi_1' = \psi_2, \quad \psi_2' = \psi_3, \quad \psi_3' = f(\psi_1, \psi_2, \psi_3, \beta),$$
 (9)

where $\psi_1 = h$, $\psi_2 = h'$, $\psi_3 = h''$, and

$$f(\psi_1, \psi_2, \psi_3, \beta) = \frac{K}{S\psi_1^3} + \frac{c}{S\psi_1^2} - \frac{1}{2S\psi_1} - \psi_2 - \frac{\beta\psi_3}{\psi_1^3}.$$

The system may be linearized at an equilibrium (constant) solution $h=h_e$,

$$\Psi' = A_{\beta,J}\Psi \tag{10}$$

where

$$A_{\beta,J} = \begin{bmatrix} 0 & 1 & 0 \\ 0 & 0 & 1 \\ J & -1 & -\frac{\beta}{Sh^2} \end{bmatrix}, \quad J = -\frac{3K}{Sh_e^4} - \frac{2c}{Sh_e^3} + \frac{1}{2Sh_e^2}. \tag{11}$$

When $\beta=0$, $A_{\beta,J}$ realizes a Hopf bifurcation if and only if J=0, which occurs provided $h_e=\sqrt{-2K}$; the corresponding eigenvalues are 0 and $\pm i$.

Next, define

$$F(\beta, h_e, \Psi) = (\psi_2, \psi_3, f_{\beta}(\psi_1 + h_e + h_H, \psi_2, \psi_3)), \tag{12}$$

where $\Psi=(\psi_1,\psi_2,\psi_3)$ and $h_H:=\sqrt{-2K}$, and consider the problem

$$\frac{d\Psi}{dt} = F(\beta, h_e, \Psi). \tag{13}$$

Given the regularity of f in a neighborhood of the degenerate Hopf bifurcation, the existence of asymptotic solutions to (13) near $\beta = 0$ and $h_e = h_H$ may be demonstrated using β and h_e as continuation parameter and applying the result of [30].

Once we have chosen the correct coordinates in which to bifurcate, these asymptotic solutions may be constructed using the work of Langford [39] and are given by

$$\Psi(s,\varepsilon) = \varepsilon[x\Phi_0(s) + y\overline{c}] + \varepsilon^2 w(s) + \mathcal{O}(\varepsilon^3),$$

$$h_e(\varepsilon) = v\varepsilon,$$

$$\beta(\varepsilon) = \varepsilon\mu + \mathcal{O}(\varepsilon^2),$$

$$T(\varepsilon) = 2\pi + \mathcal{O}(\varepsilon^2),$$
(14)

where

$$\Phi_0(s) = \sqrt{\frac{2}{3}} (-\sin s, \cos s, \sin s)^T,$$
(15a)

$$\vec{c} = (0, 0, 1)^T, \quad |\mu| < 1, \quad \nu = \pm 1,$$
 (15b)

$$w \in N(L)^{\perp}, \quad L = \frac{d}{ds} - A_{0,0},$$
 (15c)

and

$$x = \sqrt{-3(\mu^2 - 1)}, \quad y = \mu - \nu.$$
 (16)

Though one may expect to take c as a bifurcating, or continuation, parameter, the structure of (7) actually makes construction of the asymptotic solutions via [39] impossible as the system is not sufficiently smooth in c (due to the appearance of \sqrt{c}), thus motivating use of h_e as a continuation parameter here.

A comparison of these asymptotic results with the numerical results is shown in Fig. 6 for Eq. (2). Solutions were calculated for a fixed Hopf thickness h_e and for a variety of values for β ; both the predicted amplitude and the mean thickness of the resulting solution are in excellent agreement between the asymptotics and the numerics. The agreement was checked for other values of h_e and degrades as one moves further down the periodic branch away from the Hopf as can be expected.

The same asymptotic procedure may be applied to Eq. (1); these solutions are given as in (14) with Φ_0 , \vec{c} , μ , ν , and w as before and with

$$x = \sqrt{3\nu^2 - \frac{\sqrt[3]{6}}{8\sqrt[3]{K^2}}}\mu^2, \quad y = -\nu - \frac{1}{2\sqrt[3]{6K}}\mu. \tag{17}$$

Similar agreement between asymptotics and numerics was found for Eq. (1) as well (not shown).

5. Stability far from Hopf bifurcations: numerics

We next study the stability of traveling wave solutions to Eqs. (1)–(6). A refined stability analysis has been conducted for

many other PDEs like, e.g., the Allen–Cahn equation, the mKdV equation, the Kuramoto–Sivashinsky equation, or in reaction–diffusion equations; see, e.g., [40–49]. In many of these cases listed here, the nature of the nonlinearities present in the model allows an in depth ODE analysis to prescribe the structure of the traveling waves. However, the types of nonlinearities present in the long-wave models (4)–(6) make analytical tools somewhat difficult to apply, and so we turn to numerical methods for exploring the stability of solutions to *all* of the model equations; the stability of solutions to thin-film Eqs. (1)–(3) near the Hopf will be studied analytically in the next section.

The method used here for studying the stability of traveling wave solutions is described in detail in [25] and is summarized briefly here for Eq. (2). In the traveling reference frame Z=z-ct, substituting h(z,t)=Q(z-ct)+w(t,z-ct) and retaining linear terms results in

$$w_t - L_{c,Ker}w = 0 (18)$$

with

$$L_{c,Ker} = -SQ^{3}\partial_{Z}^{4} - 3SQ^{2}Q'\partial_{Z}^{3} - SQ^{3}\partial_{Z}^{2}$$

$$- [Q + 3SQ^{2}Q' - c + 3SQ^{2}(Q' + Q''')]\partial_{Z}$$

$$- [Q' + 3S(Q^{2}(Q' + Q'''))'].$$
(19)

With the separation of variables

$$w(Z,t) = e^{\lambda t} \psi(Z) \tag{20}$$

Eq. (19) is an eigenvalue problem for λ ; these eigenvalues are found numerically. To improve the accuracy of the solutions computed in AUTO, the Newton solver 'nsoli' is used in Matlab to refine Q(Z). This refined solution is then used in a pseudospectral implementation of Hill's method in Matlab; see [25] for more details of the method. The same approach was used for each of (1)–(6).

As we will discuss the linear stability near the Hopf bifurcation later, we record here that for (1), we have

$$L_{c,Fr} = -SQ^{3}\partial_{Z}^{4} - 3SQ^{2}Q'\partial_{Z}^{3} - SQ^{3}\partial_{Z}^{2}$$

$$- [2Q^{2} + 3SQ^{2}Q' - c + 3SQ^{2}(Q' + Q''')]\partial_{Z}$$

$$- [4QQ' + 3S(Q^{2}(Q' + Q'''))']. \tag{21}$$

Similar formulae can be derived for linearized versions of each of the models (1)–(6).

A family of solutions to Eq. (2) with fixed mean thickness $h_0 = 1$, period 8π , and a range of S values is shown in Fig. 7. For small S, solutions are weakly unstable, where one or more pairs of complex conjugate eigenvalues has small positive real part. These eigenvalues with positive real part represent an instability akin to the flat-film instability and are a result of having a sufficiently long domain. As S increases, however, these eigenvalues move to the left, eventually crossing the imaginary axis; for S greater than this critical value, all solutions appear to be stable, with all eigenvalues (except for the zero eigenvalue present in all solutions) containing negative real part. Thus large S can stabilize these solutions, and the critical S at which stability is reached increases with increasing period. For period less than 4π , all solutions were found to be stable, presumably due to a lack of room in the domain for a flat-film type instability to be present. Qualitatively similar results were found for (1) as well and are shown in Fig. 8 for fixed period and Fig. 9 for fixed S. The critical S at which stability is reached is shown in Fig. 10 as a function of period.

Next, we study how the stability changes in the corresponding long-wave model solutions. The stability of solutions to Eq. (4) was studied in [25], and it was shown that lower branch (small-amplitude) solutions were weakly unstable with one or more

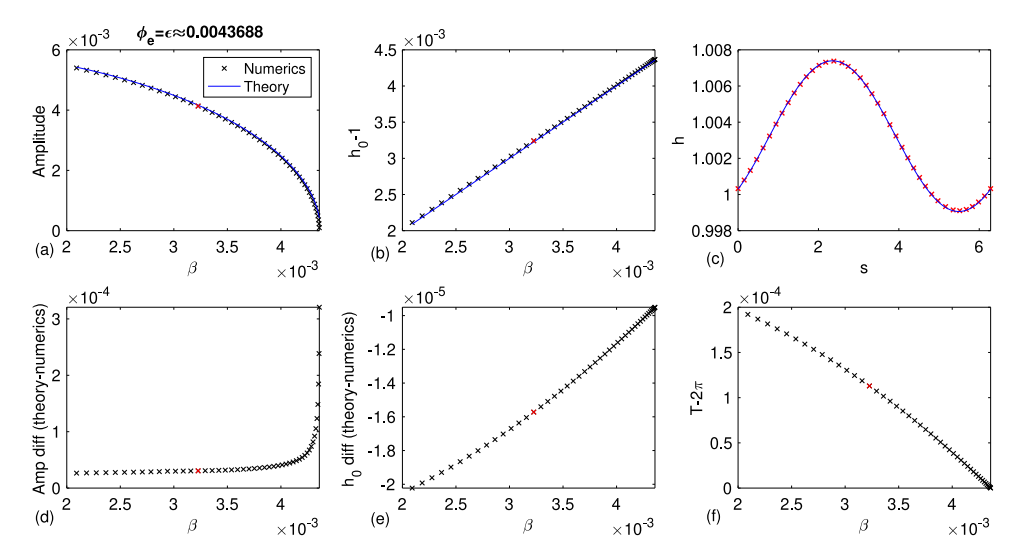


Fig. 6. (a) Amplitude and (b) mean thickness (deviation from 1) of numerical (black x's) and asymptotic (blue line) periodic solutions to (2) coming from a Hopf bifurcation occurring at $h_0 - 1 = h_e \approx 0.0043688$. (c) Profile of solution corresponding to red x in (a,b). (d,e) Difference between numerics and theory in panels (a,b), respectively. (f) Increase in period from Hopf period of 2π . (For interpretation of the references to color in this figure legend, the reader is referred to the web version of this article.)

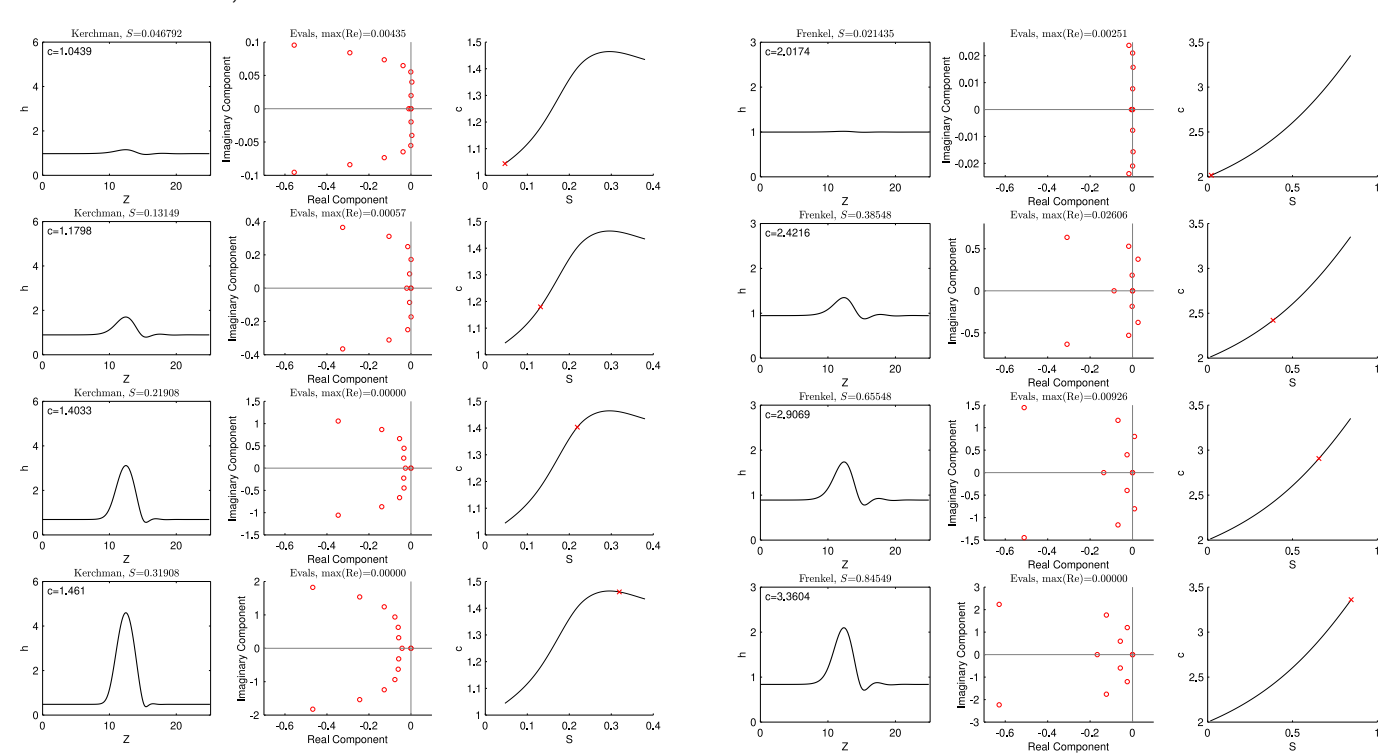


Fig. 7. Traveling wave solutions and linearized spectrum around those solutions to (2) with mean thickness $h_0=1$ and period 8π for (top row) $S\approx 0.05$, (second row) $S\approx 0.13$, (third row) $S\approx 0.22$, and (bottom row) $S\approx 0.32$. Only eigenvalues with largest real part are shown; the maximum real part of the eigenvalues is listed to five decimal places. Red ×'s in third column corresponds to parameter values of solutions shown.

pairs of complex-conjugate eigenvalues containing small positive real parts, while upper branch (large-amplitude) solutions were unstable with one large, positive real eigenvalue. For Eq. (5), each family of solutions examined with fixed \tilde{S} , h_0 and period was either stable or weakly unstable.

Are solutions to Eq. (6) stable? As with (4), the answer depends on the branch of solutions considered. Fig. 11 shows the linearized spectrum of several solutions lying along one of the families shown in Fig. 5. For very thin films, only small-amplitude

Fig. 8. Same as Fig. 7 but for solutions to (1). (Top row) $S \approx 0.02$, (second row) $S \approx 0.39$, (third row) $S \approx 0.66$, and (bottom row) $S \approx 0.85$.

solutions are found, and these are stable due to the period being small enough to prevent any flat-film type instability. As one moves further up the branch of solutions, a turnaround, or fold, point is reached, similar to that found for (4) in [10,25]. As one passes through this turnaround point, one real eigenvalue changes sign from negative to positive. Moving further along this 'middle' branch of solutions, this positive real eigenvalue grows until reaching some maximum, after which it begins to return to zero. It crosses zero at a second turnaround point, and solutions lying on this 'upper' branch are stable. This second turnaround point does not exist in families of solutions to (4) and may be attributed to the core flow's role in saturating wave growth

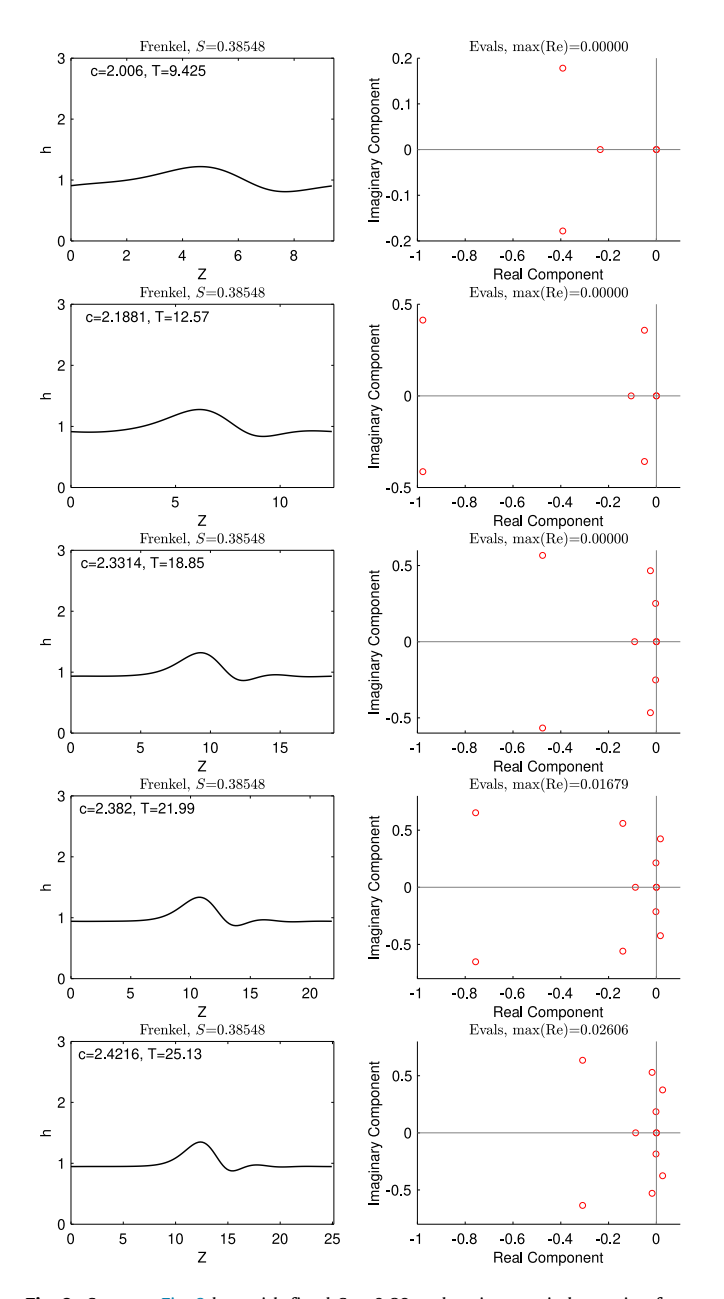


Fig. 9. Same as Fig. 8 but with fixed S pprox 0.39 and various periods ranging from $T pprox 3\pi$ to 8π .

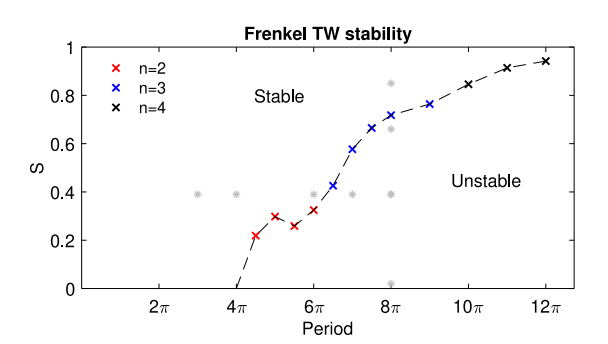


Fig. 10. Regions of *S*-period parameter space where single-hump traveling wave solutions to (1) with $h_0=1$ are stable or unstable. Color indicates which eigenvalue has real part of zero at these critical *S* values. Light gray asterisks denote solutions shown in Figs. 8 and 9.

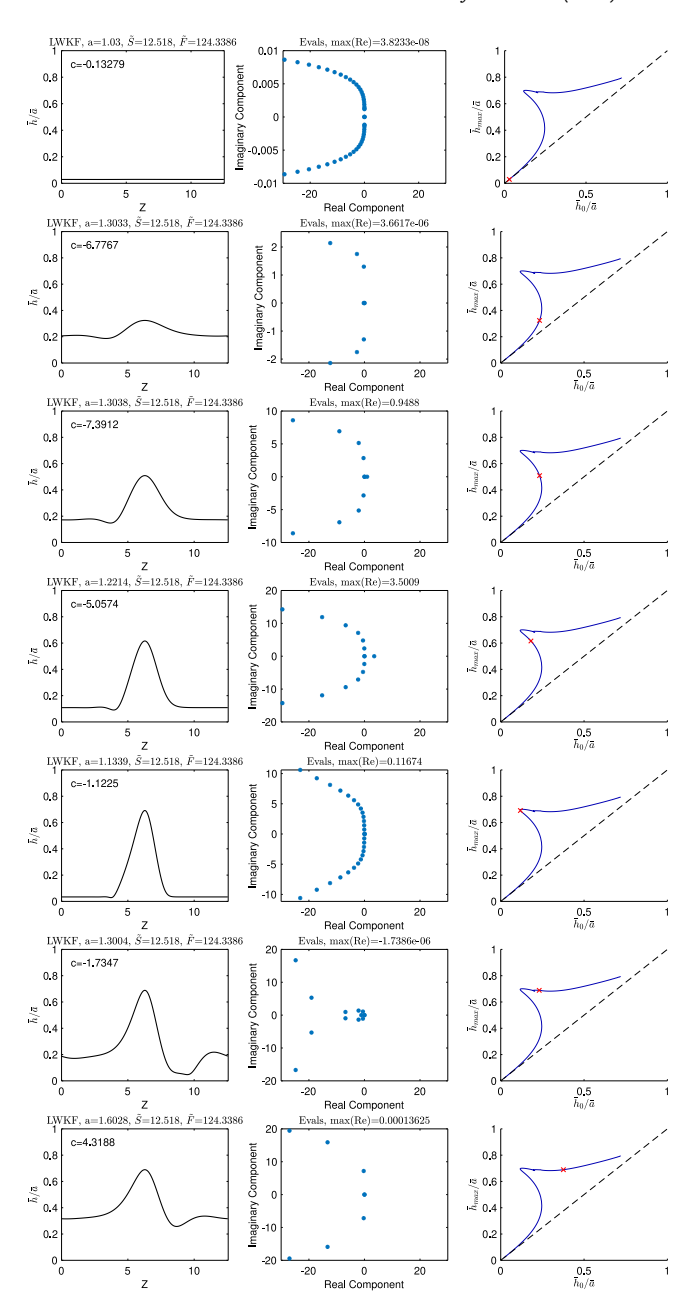


Fig. 11. Traveling wave solutions and linearized spectrum around those solutions to (6) with mean thickness $h_0=1$, $\bar{S}\approx 12.5$, $\bar{F}\approx 124.3$, and period 4π for various values of a. Only eigenvalues with largest real part are shown; the maximum real part of the eigenvalues is listed. Red ×'s in third column corresponds to parameter values of solutions shown. (For interpretation of the references to color in this figure legend, the reader is referred to the web version of this article.)

for thick films. Thus the upper branch reflects the structure of solutions to (5) as the core flow terms asymptotically dominate the gravity terms for thick films along this upper branch, while the middle and lower branches reflect the structure of solution families for (4). Note also that the velocity changes sign from negative to positive along the upper branch as a critical thickness is reached where the core flow begins to dominate the effects of gravity in the competition to determine the direction of the wave's propagation. At this threshold the wave profile reverses orientation to reflect this change (i.e., the trough leads the crest, and moves from the left of the wave crest to the right as one increases film thickness along the upper branch of solutions).

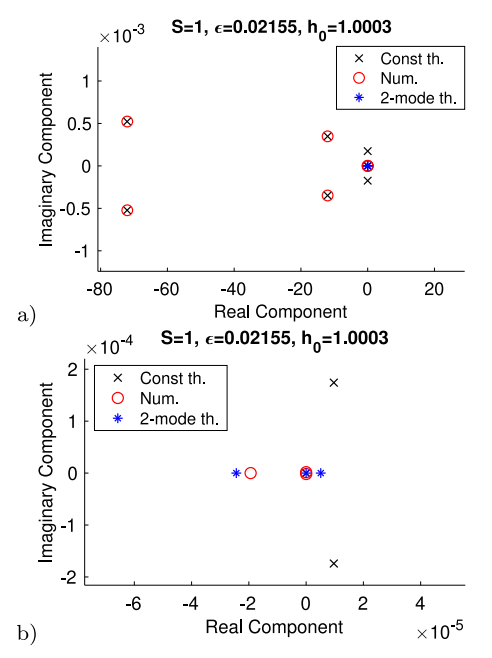


Fig. 12. (a) Spectrum of a traveling wave solution to (2) with S=1 near the Hopf bifurcation. Numerically computed spectrum (red circles) and constant theory spectrum according to (22) (black \times 's) are shown; 2-mode theory eigenvalues (see Eq. (24)) near zero are also shown. (b) Same as (a) but zoomed in around 0.

6. Stability near Hopf bifurcations in thin film models: multimode asymptotics

We first seek to understand the stability of traveling wave solutions to (2) by examining the spectrum of the linearized operator $L_{c,Ker}$ with periodic boundary conditions near the Hopf bifurcation at $\beta=0$ and $Q=h_e$ using asymptotics; we begin by noting that $L_{c,Ker}$ from (19) has linear spectrum

$$\left\{ -SQ^{3} \left(\left(\frac{n}{T} \right)^{2} - 1 \right) \left(\frac{n}{T} \right)^{2} - i(Q - c) \frac{n}{T} : n \in \mathbb{Z} \right\}. \tag{22}$$

From (22) it is clear that at the Hopf bifurcation, where Q-c=0, the spectrum is real. For $T\leq 2\pi$, $\mathrm{Re}\,\lambda\leq 0$, while for $T>2\pi$ there are eigenvalues to the right of the imaginary axis. Fig. 12(a) shows the eigenvalues predicted by this constant theory (black ×'s) for a traveling wave solution to (2) near the Hopf bifurcation. The agreement between numerics and constant theory is excellent for $n=0,2,3,\ldots$; for n=1, however, the numerically computed eigenvalues are much closer to zero than expected from the theory.

To investigate the discrepancy of near-zero eigenvalues near the Hopf bifurcation, we will use what we call a two-mode system. Multi-mode expansions of this type have appeared in studying periodic traveling waves before, for instance in KdV and related systems [50,51]. When Q-c=0, $\lambda=0$ is an eigenvalue of $L_{c,Ker}$ of multiplicity three. Furthermore, since Q solves the nonlinear problem, Q' is a nearby kernel element of $L_{c,Ker}$. In the perturbation, $L_{c,Ker,\varepsilon}$ this ensures that $\cos\left(\frac{x}{T}\right)$ is (to order ε) in the kernel of $L_{c,Ker,\varepsilon}$, so a higher order perturbation should be used. We use the first and second Fourier modes to define the perturbed operator $\tilde{L}_{c,Ker}$ given by replacing Q by

$$Q + \sum_{k=1}^{2} \varepsilon_k \sin(kx/T + \varphi_k)$$

in $L_{c,Ker}$, where ε_k and φ_k are numerically computed for $1 \le k \le 2$.

Letting

$$\langle u, v \rangle = \frac{1}{2\pi T} \int_0^{2\pi T} u \bar{v} \, dx \tag{23}$$

define an inner product on $L^2_{per}([0,2\pi T])$, and defining the vector space

$$V = \text{span}\{v_1 = e^{-ix/T}, v_2 = 1, v_3 = e^{ix/T}, v_4 = e^{-2ix/T}, v_5 = e^{2ix/T}\}.$$

we then focus on the map $\phi:V\to\mathbb{R}^5$ as the linear operator defined by $\phi(v_k)=e_k,\,1\leq k\leq 5$, where $\{e_k\}_{k=1}^5$ is the standard basis of \mathbb{R}^5 . Next, let $M:\mathbb{R}^5\to\mathbb{R}^5$ be the matrix defined by

$$M = \left[m_{jk} \right] \tag{24}$$

where $m_{jk} = \langle \tilde{L}_{c,Ker} v_j, v_k \rangle$. This matrix is a representation of the operator $P \circ \tilde{L}_{c,Ker}$, where P is the projection from $L^2_{per}([0, 2\pi T])$, the space of square-integrable periodic functions, to V. Studying this matrix gives insight into the spectrum of $L_{c,Ker}$ when Q - c is comparatively small to ε . Interestingly, this matrix has a strongly negative movement of one of the zero eigenvalues.

Fig. 12(b) shows the near-zero eigenvalues computed numerically (red circles) and predicted by the higher-order two-mode system (blue asterisks). The agreement is significantly better than with the constant theory; in particular, the negative movement of one of the zero eigenvalues is in good agreement with the numerical calculations. Given that we have increased our system size to attempt to overcome the issue of degeneracy near 0, there is a small positive real eigenvalue predicted by the higher-order theory that is not seen in the numerically calculated eigenvalues. The behavior near zero requires further analysis, but overall the agreement between the higher-order asymptotic theory and numerics appears to be reasonable.

In a similar fashion, the stability of solutions to (1) can be studied by examining the spectrum of $L_{c,Fr}$ given in (21). The spectrum of the constant problem is

$$\left\{-SQ^3\left(\left(\frac{n}{T}\right)^2-1\right)\left(\frac{n}{T}\right)^2-i(2Q^2-c)\frac{n}{T}:n\in\mathbb{Z}\right\}.$$
 (25)

Once again, agreement between the constant theory and numerics is excellent for $n=0,2,3,\ldots$ but not for n=1 (not shown). The two-mode theory discussed above can be applied again to investigate this discrepancy, and the results show a qualitatively similar strongly negative movement of one of the zero eigenvalues which is again in good agreement with numerics (not shown).

7. Conclusions

Traveling wave solutions have been explored asymptotically and numerically for two classes of models for falling film flows inside a tube and for core-annular flows. Asymptotics, making use of the work of [39], were used to provide justification for the smoothing technique used to find traveling wave solutions numerically for these models. A numerical exploration of solutions to one of the long-wave models revealed solution families with multiple turning points arising from the interplay between gravity, pressure-driven core flow, viscosity, and surface tension. The stability of traveling wave solutions to the thin-film models was explored using asymptotics near the Hopf bifurcation. A simple theory based on the constant solution at the Hopf point predicted all but two of the eigenvalues very well; for these two eigenvalues near zero, higher-order asymptotics were required to produce good agreement with numerics. Far from the Hopf bifurcation, the stability of traveling wave solutions was explored

numerically, and changes in stability corresponding to turning points in solution families were shown.

We note that the current study has focused entirely on singlehump traveling wave solutions which occur most frequently in numerical simulations, and are seen most readily in thin-film experiments. Other solutions, including multiple-hump solutions, have been neglected here, and it would be interesting to explore differences in stability for different types of solutions in the future.

Declaration of competing interest

The authors declare that they have no known competing financial interests or personal relationships that could have appeared to influence the work reported in this paper.

Acknowledgments

J.L.M. and S.S. acknowledge support from the NSF through NSF CAREER Grant DMS-1352353. R.C. and H.R.O. acknowledge support from the NSF, USA through RTG DMS-0943851, CMG ARC-1025523, DMS-1009750. R.C. also acknowledges support from the NSF, USA through DMS-1517879, DMS-1910824, and DMS-1909521; the NIH, USA through NIEHS 534197-34; and the ONR, USA through ONR N00014-18-1-2490.

References

- [1] R.V. Craster, O.K. Matar, Dynamics and stability of thin liquid films, Rev. Modern Phys. 81 (2009) 1131–1198.
- [2] S.L. Goren, The instability of an annular thread of fluid, J. Fluid Mech. 27 (1962) 309–319.
- (1962) 309–319.[3] C. Hickox, Instability due to viscosity and density stratification in axisymmetric pipe flow, Phys. Fluids 14 (1971) 251–262.
- [4] C.-S. Yih, Instability due to viscosity stratification, J. Fluid Mech. 27 (1967) 337–352.
- [5] M.N.J. Moore, Stratified Flows with Vertical Layering of Density (Diss.), University of North Carolina, 2010.
- [6] A.L. Frenkel, Nonlinear theory of strongly undulating thin films flowing down vertical cylinders, Europhys, Lett. 18 (1992) 583–588.
- [7] V. Kerchman, Strongly nonlinear interfacial dynamics in core-annular flows, J. Fluid Mech. 772 (1995) 569–599.
- [8] R.V. Roy, A.J. Roberts, M.E. Simpson, A lubrication model of coating flows over a curved substrate in space, J. Fluid Mech. 454 (2002) 235–261.
- [9] R. Camassa, M.G. Forest, L. Lee, H.R. Ogrosky, J. Olander, Ring waves as a mass transport mechanism in air-driven core-annular flows, Phys. Rev. E 86 (2012) 066305–1–11.
- [10] R. Camassa, H.R. Ogrosky, J. Olander, Viscous film flow coating the interior of a vertical tube. Part I. Gravity-driven flow, J. Fluid Mech. 745 (2014) 682–715.
- [11] R. Camassa, H.R. Ogrosky, J. Olander, Viscous film flow coating the interior of a vertical tube. Part II. Air-driven flow, J. Fluid Mech. 825 (2017) 1056–1090.
- [12] S.P. Lin, Finite amplitude side-band stability of a viscous film, J. Fluid Mech. 63 (1974) 417–429.
- [13] S.P. Lin, W.C. Liu, Instability of film coating of wires and tubes, AIChE J. 24 (1975) 775–782.
- [14] R. Camassa, H.R. Ogrosky, On viscous film flows coating the interior of a tube: thin-film and long-wave models, J. Fluid Mech. 772 (2015) 569–599.
- [15] N.J. Balmforth, G.R. Ierley, E.A. Spiegel, Chaotic pulse trains, SIAM J. Appl. Math. 54 (1994) 1291–1334.
- [16] C. Duprat, F. Giorgiutti-Dauphiné, D. Tseluiko, S. Saprykin, S. Kalliadasis, Liquid film coating a fiber as a model system for the formation of bound states in active dispersive-dissipative nonlinear media, Phys. Rev. Lett. 103 (2009) 234501-1-234501-4.
- [17] C. Elphick, G.R. Ierley, O. Regev, E.A. Spiegel, Interacting localized structures with Galilean invariance, Phys. Rev. A 44 (1991) 1110–1122.
- [18] M. Pradas, D. Tseluiko, S. Kalliadasis, Rigorous coherent-structure theory for falling liquid films: viscous dispersion effects on bound-state formation and self-organization, Phys. Fluids 23 (2011) 044104–1–044104–19.
- [19] D. Tseluiko, S. Saprykin, C. Duprat, F. Giorgiutti-Dauphiné, S. Kalliadasis, Pulse dynamics in low-Reynolds-number interfacial hydrodynamics: Experiments and theory, Physica D 239 (2010) 2000–2010.

- [20] D. Tseluiko, S. Kalliadasis, Weak interaction of solitary pulses in active dispersive-dissipative nonlinear media, IMA J. Appl. Math. 79 (2014) 274–299.
- [21] C. Ruyer-Quil, P. Manneville, Improved modeling of flows down inclined planes, Eur. Phys. J. B 6 (1998) 277–292.
- [22] C. Ruyer-Quil, P. Treveleyan, F. Giorgiutti-Dauphiné, C. Duprat, S. Kalliadasis, Modelling film flows down a fibre, J. Fluid Mech. 603 (2008) 431-462.
- [23] C. Ruyer-Quil, S. Kalliadasis, Wavy regimes of film flow down a fiber, Phys. Rev. E 85 (2012) 046302–1–046302–23.
- [24] R. Camassa, L. Lee, in: A. Chwang, M. Teng, D. Valentine (Eds.), Advances in Engineering Mechanics - Reflections and Outlooks, World Scientific, 2006, pp. 222–238.
- [25] R. Camassa, J.L. Marzuola, H.R. Ogrosky, N. Vaughn, Traveling waves for a model of gravity-driven film flows in cylindrical domains, Physica D 333 (2016) 254–265.
- [26] R.V. Craster, O.K. Matar, On viscous beads flowing down a vertical fibre, J. Fluid Mech. 553 (2006) 85–105.
- [27] S. Kalliadasis, H.-C. Chang, Drop formation during coating of vertical fibers, J. Fluid Mech. 261 (1994) 135–168.
- [28] V.I. Kerchman, A.L. Frenkel, Interactions of coherent structures in a film flow: Simulations of a highly nonlinear evolution equation, Theor. Comput. Fluid Dyn. 6 (1994) 235–254.
- [29] I.L. Kliakhandler, S.H. Davis, S.G. Bankoff, Viscous beads on vertical fibre, J. Fluid Mech. 429 (2001) 381–390.
- [30] M. Shearer, Coincident bifurcation of equilibrium and periodic solutions of evolution equations, J. Math. Anal. Appl. 84 (1991) 113–132.
- [31] P.S. Hammond, Nonlinear adjustment of a thin annular film of viscous fluid surrounding a thread of another within a circular cylindrical pipe, J. Fluid Mech. 137 (1983) 363–384.
- [32] J.M. Hyman, B. Nicolaenko, The Kuramoto-Sivashinsky equation: A bridge between PDE's and dynamical systems, Physica D 18 (1986) 113–126.
- [33] J.M. Hyman, B. Nicolaenko, S. Zaleski, Order and complexity in the Kuramoto-Sivashinsky model of weakly turbulent interfaces, Physica D 23 (1986) 265–292.
- [34] G.I. Sivashinsky, D.M. Michelson, On irregular wavy flow of a liquid down a vertical plane, Progr. Theoret. Phys. 63 (1980) 2112–2114.
- [35] T. Pernas-Castaño, J.J.L. Velázquez, Analysis of a thin film approximation for two-fluid Taylor-Couette flows, 2019, pre-print. arXiv:1905.13606.
- [36] M.A. Johnson, P. Noble, L.M. Rodrigues, K. Zumbrun, Spectral stability of periodic wave trains of the Korteweg-de Vries/Kuramoto-Sivashinsky equation in the Korteweg-de Vries limit, Trans. Amer. Math. Soc. 367 (3) (2015) 2159–2212.
- [37] E. Doedel, B. Oldeman, et al., AUTO-07P, Software Package and User Manual.
- [38] J.F. Dietze, G. Lavalle, C. Ruyer-Quil, Falling liquid films in narrow tubes: occlusion scenarios, J. Fluid Mech. 894 (2020) A17-1-44.
- [39] W.F. Langford, Periodic and steady-state mode interactions lead to tori, J. Appl. Math. 37 (1) (1979) 22-48.
- [40] B. Barker, M.A. Johnson, P. Noble, L.M. Rodrigues, K. Zumbrun, Stability of viscous St. Venant roll-waves: from onset to the infinite-Froude number limit, 2015, pre-print. arXiv:1503.01154.
- [41] J. Bronski, M. Johnson, T. Kapitula, An index theorem for the stability of periodic travelling waves of Korteweg-de Vries type, Proc. Roy. Soc. Edinburgh Sect. A 141 (2011) 1141–1173.
- [42] C.W. Curtis, B. Deconinck, On the convergence of Hill's method, Math. Comp. 79 (2010) 169–187.
- [43] B. Deconinck, J.N. Kutz, Computing spectra of linear operators using the Floquet–Fourier-Hill method, J. Comput. Phys. 219 (2006) 296–321.
- [44] B. Deconinck, M. Nivala, The stability analysis of the periodic traveling wave solutions of the mKdV equation, Stud. Appl. Math. 126 (2011) 17–48.
- [45] D. Ginsberg, G. Simpson, Analytical and numerical results on the positivity of steady state solutions of a thin film equation, DCDS-B 18 (5) (2013) 1305–1321.
- [46] R.S. Laugesen, M.C. Pugh, Energy levels of steady states for thin-film-type equations, J. Differential Equations 182 (2) (2002) 377-415.
- [47] R.S. Laugesen, M.C. Pugh, Linear stability of steady states for thin film and Cahn-Hilliard type equations, Arch. Ration. Mech. Anal. 154 (1) (2000) 3–51.
- [48] B. Nicolaenko, B. Scheurer, R. Temam, Some global dynamical properties of the kuramoto-sivashinsky equations: nonlinear stability and attractors, Physica D 16 (1985) 155–183.
- [49] B. Sandstede, A. Scheel, Absolute and convective instabilities of waves on unbounded and large bounded domains, Physica D 145 (2000) 233–277.
- [50] J. Bronski, M. Johnson, The modulational instability for a generalized Korteweg-de Vries equation, Arch. Ration. Mech. Anal. 197 (2) (2010) 357-400
- [51] M. Haragus, T. Kapitula, On the spectra of periodic waves for infinite-dimensional Hamiltonian systems, Physica D 237 (20) (2008) 2649–2671.